Reinventing the Wheel:
The Chaotic Sandwheel

Anthony Tongen and Roger J. Thelwell

Department of Mathematics and Statistics, James Madison University

David Becerra-Alonso

Department of Management and Quantitative Methods,

Universidad Loyola Andalucia

to appear in the American Journal of Physics

(Dated: July 12, 2012)

Abstract

The Malkus chaotic waterwheel, a tool to mechanically demonstrate Lorenzian dynamics, motivates the study of a chaotic sandwheel. We model the sandwheel in parallel with the waterwheel when possible, noting where methods may be extended and where no further analysis seems feasible. Numerical simulations are used to compare and contrast the behavior of the sandwheel with the waterwheel. Simulations confirm that the sandwheel retains many of the elements of chaotic Lorenzian dynamics. However, bifurcation diagrams show dramatic differences in where the order-chaos-order transitions occur.

PACS numbers: 45.20.D-, 45.20.da, 45.20.dc, 45.20.df

Keywords: Malkus' Waterwheel, Lorenzian dynamics, Sandwheel

I. INTRODUCTION

The Lorenz equations are a well-known and well-studied system of equations that exhibit chaos. Originally posed to capture features of atmospheric convection,[1] the system has also been shown to model a variety of physical applications including lasers and dynamos.[2,3] In 1972, Willem Malkus developed the *chaotic waterwheel*, a mechanical system for which the Lorenz equations serve as a mathematical model.[4] The chaotic waterwheel has been popularized by Strogatz;[5] it consists of a disk with punctured cups equally spaced around its circumference and driven by a single source of water. Two control parameters, the water inflow rate and the rotational friction, allow the system to exhibit a wide range of behaviors. Numerous authors have built upon the work of Malkus.[6–12]

The Malkus waterwheel was carefully designed to simulate the Lorenz equations, and so there is no *a priori* expectation that a change in media will lead to similar (or dissimilar) dynamics. This article will focus on the novel change of the media in the wheel from water to sand. Mathematically, the use of sand (or any other granular material) leads to a slight modification of the original model. Consider two containers, one filled with water and the other with sand. The pressure head with water obeys a linear scaling, but is largely constant for sand. Thus, the rate equation for water mass is given by $dm/dt = -K_w m$, where m is the mass in an individual cup and K_w is the outflow rate of the water. In contrast, the rate equation for the sand mass from a non-empty container is modeled by $dm/dt = -K_s$, where K_s is the leakage rate of the sand. Note that the units of K_s $(kg \cdot s^{-1})$ differ from those of K_w (s^{-1}).

This slight modification brings about signifiant differences in both the analytical derivation and the numerical results. Unlike the waterwheel, where mathematical equations motivated the physical experiment, in this case a physical sandwheel experiment was used to motivate the mathematical analysis. In the Summer of 2009, a group of students built a chaotic sandwheel—the first that we are aware of—in the first weeks of a summer research experience. Figure 1 provides a schematic of the sandwheel. The project succeeded in piquing the interest of the students involved, who quickly paralleled the mathematical analysis of the waterwheel for the sandwheel. The experimental aspects of constructing the sandwheel and making accurate measurements proved to be quite a challenge, and the difficulties quickly convinced our students to focus on the mathematical analysis. Therefore, the functioning sandwheel served more as a motivation for the mathematics than as a viable experimental playground, and a true experimental-grade sandwheel remains an intriguing open problem.

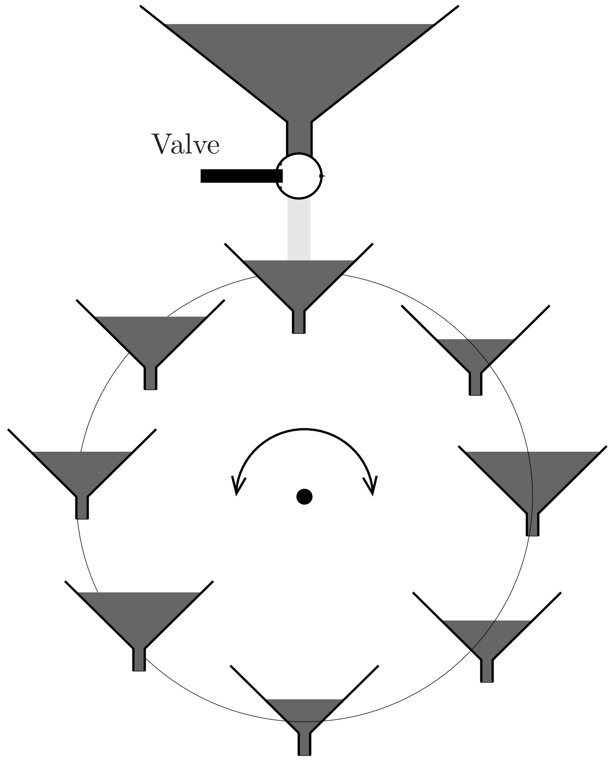

FIG. 1: A schematic of the experimental sandwheel.

Nevertheless, the construction of the sandwheel and the measurements we made provided the insights necessary for what follows in this article, beginning with the basic notion of leakage rate and its consequences. Intuitively, the constant rate of sand loss would appear to make the analysis of the problem easier. In fact, the problem becomes much harder to analyze. No longer is the leakage rate (per cup) proportional to the mass, but is instead nonlinear; it is a constant that switches to zero when the cup is empty. Unfortunately, this means that the continuous mathematical analysis typically applied to the waterwheel cannot be applied to the sandwheel.

We develop the analysis of the sandwheel in parallel with that of the waterwheel when possible, noting where methods may be extended and where no further analysis seems feasible. Numerical simulations are then used to explore the behavior of the sandwheel. We compare and contrast the behavior of the sandwheel with the waterwheel, classifying the behavior using center of mass dynamics. Numerical simulations verify that the sandwheel retains many of the elements needed for chaotic Lorenzian dynamics. However, bifurcation diagrams show dramatic differences in where the order-chaos-order transitions occur.

II. MATHEMATICAL MODELING

To begin to understand the differences that arise between the waterwheel and sandwheel, we follow the analysis of Matson[10] and consider tracking the individual cups to describe the motion. Notationally, we will use subscripts of w and s to distinguish variables in the waterwheel and the sandwheel, respectively. We assume that cups on the waterwheel leak at a rate K_w, proportional to the mass contained in each of the N cups, and that the frictional force is proportional to the rotational speed of the wheel. We will also assume that cups do not overflow. With these assumptions, the system of differential equations describing the waterwheel is

$$\frac{dm_i}{dt} = Q(\theta_i) - K_w m_i, \tag{1}$$

where m_i is the mass of the i^{th} cup ($i = 1 \ldots N$), and

$$Q(\theta_i) = \begin{cases} Q, & \text{if } \cos(\theta_i) \geq \cos(\pi/N) \\ 0, & \text{otherwise} \end{cases} \tag{2}$$

is the inflow rate per cup i as a function of the cup's angular position θ_i. The solution for each cup i is then

$$m_i(t) = \frac{Q(\theta_i)}{K_w} + e^{-K_w t}\left(m_i(0) - \frac{Q(\theta_i)}{K_w}\right), \tag{3}$$

so long as the inflow $Q(\theta_i)$ is constant. Notice that the long term mass in a cup will approach a constant, even if $Q(\theta_i)$ does not change to zero.

Using the same assumptions for the sandwheel, with the exception that sand demonstrates a constant leakage rate K_s, we find a system of differential equations given by

$$\frac{dm_i}{dt} = Q(\theta_i) - H(m_i)K_s, \tag{4}$$

where the Heaviside (or unit step) function obeys

$$H(x) = \begin{cases} 0, & \text{if } x < 0 \\ 1, & \text{if } x > 0 \end{cases} \tag{5}$$

and is required to conserve mass. The solution to Eq. (4) between changes of $Q(\theta_i)$ and $H(m_i)$ is given by

$$m_i(t) = m(0) + [Q(\theta_i) - K_s H(m_i)]\, t. \tag{6}$$

The difference between the mass leakage factors in Eqs. (1) and (4)—m versus $H(m)$—is at the heart of what makes the two wheels different. If $Q < K_s$ then the system drains completely to zero sand mass. On the other hand, if $Q > NK_s$ then the mass always becomes unbounded. For Q in between these limits, it is not obvious how the average outflow $K_s \sum H(m_i)$ compares with the inflow Q. Thus, when $K_s < Q < NK_s$, an analog to steady-state waterwheel mass can occur, with sandwheel mass varying (repeatedly or randomly) about a finite average.

The discrete torque balance equation, which states that the time rate of change of the system's angular momentum must balance the frictional and gravitational torque, is given by

$$I\dot{\omega} = -\nu\omega + gr\sum_{i=1}^{N} m_i \sin(\theta_i), \tag{7}$$

where r is the radius of the wheel and g is acceleration due to gravity. Angular momentum is $I\omega$, where the inertial term I is a combination of the inertia of both the wheel (I_o) and the media. The moment of inertia I, modeled by $I_0 + r^2 \sum_{i=1}^{N} m_i$, will be denoted I_w in the waterwheel setting, and by I_s in the sandwheel setting. Since the total water mass approaches a steady state, I_w will be considered a constant, while in general I_s is not. The drag parameter ν, as it is in Strogatz,[5] includes the effect of wheel shaft friction (or a brake) and the slowdown effect due to bringing the input water (or sand) up to the speed of the bucket into which it falls. Recently, Illing et. al. experimentally verified that damping can be modeled as a torque linear in velocity.[12] The addition of the equation $\dot{\theta}_1 = \omega$ closes this system in $N + 2$ equations.

A Fourier analysis of the waterwheel, as presented by Strogatz,[5] introduces a series representation for $m(\theta)$ and $Q(\theta)$. Remarkably, only the equation for the first mode needs to be considered—the zeroth mass mode approaches a steady state and all higher modes decay to zero. However, it is at this point where classic Fourier analysis fails for the sandwheel; it is no longer clear if the zeroth mass mode approaches a constant, nor is $H(m_i)$ easily amenable to analysis and subsequent dimension reduction. This discussion hints at the nonintuitive nature of the sandwheel and raises the question of whether chaos is present in the sandwheel as it is in the waterwheel.

A derivation based on the analysis of the center of mass is appealing; Matson[10] reduces the N mass dimensions of Eq. (1) down to two coordinates that provide a clear and concise way to observe system dynamics. Following suit, we introduce center of mass coordinates

$$y_{cm} = \frac{r}{M} \sum_{i=1}^{N} m_i \sin(\theta_i) \tag{8}$$

and

$$z_{cm} = \frac{r}{M} \sum_{i=1}^{N} m_i \cos(\theta_i), \tag{9}$$

where M is the total mass in the system. For water we have $M_w = Q/K_w$ at steady state, and for sand it is possibly an unbounded function in time.

For the waterwheel, differentiation of y_{cm} and z_{cm} with respect to t, and substitution of $\dot{m}_i$ from Eq. (1) yields

$$\dot{y}_{cm} = \omega z_{cm} - K_w y_{cm} \tag{10}$$

and

$$\dot{z}_{cm} = \frac{r q_0}{M_w} - \omega y_{cm} - K_w z_{cm}, \tag{11}$$

where the $\sum Q(\theta_i)\sin(\theta_i)$ term has been dropped because it is small and approaches zero for large N, and q_0, defined as $\sum Q(\theta_i)\cos(\theta_i)$, is approximately equal to Q, its value for large N.

The torque balance equation for the waterwheel turns out to be only a slight modification of Eq. (7), and is given by

$$I_w \dot{\omega} = -\nu\omega + g M_w y_{cm}. \tag{12}$$

It is worth repeating just how remarkable it is that the motion of the system, originally described by $N + 2$ equations, can be accurately described by the three variables y_{cm}, z_{cm}, and ω.

For the sandwheel, the center of mass motion cannot be as cleanly stated as in Eqs. (10) and (11). We have instead

$$\dot{y}_{cm} = -\frac{\dot{M}_s}{M_s} y_{cm} - K_s \frac{r}{M_s} \sum_{i=1}^{N} H(m_i)\sin(\theta_i) + \omega z_{cm}, \tag{13}$$

$$\dot{z}_{cm} = -\frac{\dot{M}_s}{M_s} z_{cm} - K_s \frac{r}{M_s} \sum_{i=1}^{N} H(m_i)\cos(\theta_i) - \omega y_{cm} + \frac{r q_0}{M_s}, \tag{14}$$

and

$$\dot{M}_s = \sum_{i=1}^{N} \dot{m}_i = Q - K_s \gamma(t), \tag{15}$$

where $\gamma(t) = \sum_{i=1}^{N} H(m_i)$. As discussed in the next Section, our results suggest that γ, a stepwise constant function denoting the number of cups containing sand, is an important function in the dynamics. Although deterministic, γ introduces an interesting noise-like influence.

The torque balance equation for the sandwheel is straightforward to rewrite in terms of center of mass coordinates. Unlike with the waterwheel, however, it requires knowledge of the dynamics of M_s and I_s (and therefore m_i for all cups). The analog to Eq. (12) is simply

$$I_s\dot{\omega} = -\nu\omega + gM_s y_{cm}. \tag{16}$$

Unfortunately the system that uses center of mass coordinates for the sandwheel cannot be closed as was possible for the waterwheel, because it depends upon complete knowledge of m_i for each cup. We instead are forced to consider the full mass-tracking system of $N+2$ equations. Such an analysis is carried out numerically.

III. NUMERICAL RESULTS

The behavior of these complicated discrete systems is explored through a series of numerical experiments. Using an adaptive Runge-Kutta scheme, we compute solutions $\{m_i, \theta, \omega\}$ (measured in $kg, rad, rad \cdot s^{-1}$, respectively) of the waterwheel (Eqs. [1,7]) and sandwheel (Eqs. [4,7]) systems. We also compute y_{cm} and z_{cm}, both measured in m. We consider simulations of $N = 8$ cups at radius $r = 0.2\,m$, with damping parameter $\nu = 1\,kg \cdot m^2 \cdot s^{-1}$, gravitational acceleration $g = 9.8\,m \cdot s^{-2}$, inflow $Q = 0.2\,kg \cdot s^{-1}$, and outflow either $K_w = 0.09\,s^{-1}$ or $K_s = 0.09\,kg \cdot s^{-1}$ in mks units. The initial rotational inertia I_0 is a very flexible parameter in the simulation, since it reflects the design of our hypothetical experimental apparatus. Here we choose it to be a physically reasonable value of 1 $kg \cdot m^2$ and consider Q and K values which focus analysis on the media driven dynamics rather than on momentum of the wheel. We remove transients by discarding the first 2,000 seconds of the simulation. Units will often be suppressed in the rest of the paper for simplicity.

Recall that, for a suitable choice of parameters, the classic Lorenz butterfly structure can be seen for the waterwheel when one views a 3-d parametric plot of the two Fourier coefficients and the velocity, or if one plots the two center of mass coordinates and the velocity (*e.g.* Strogatz or Matson).[5,10] Following Matson, the top panel of Fig. 2 is a projection of the

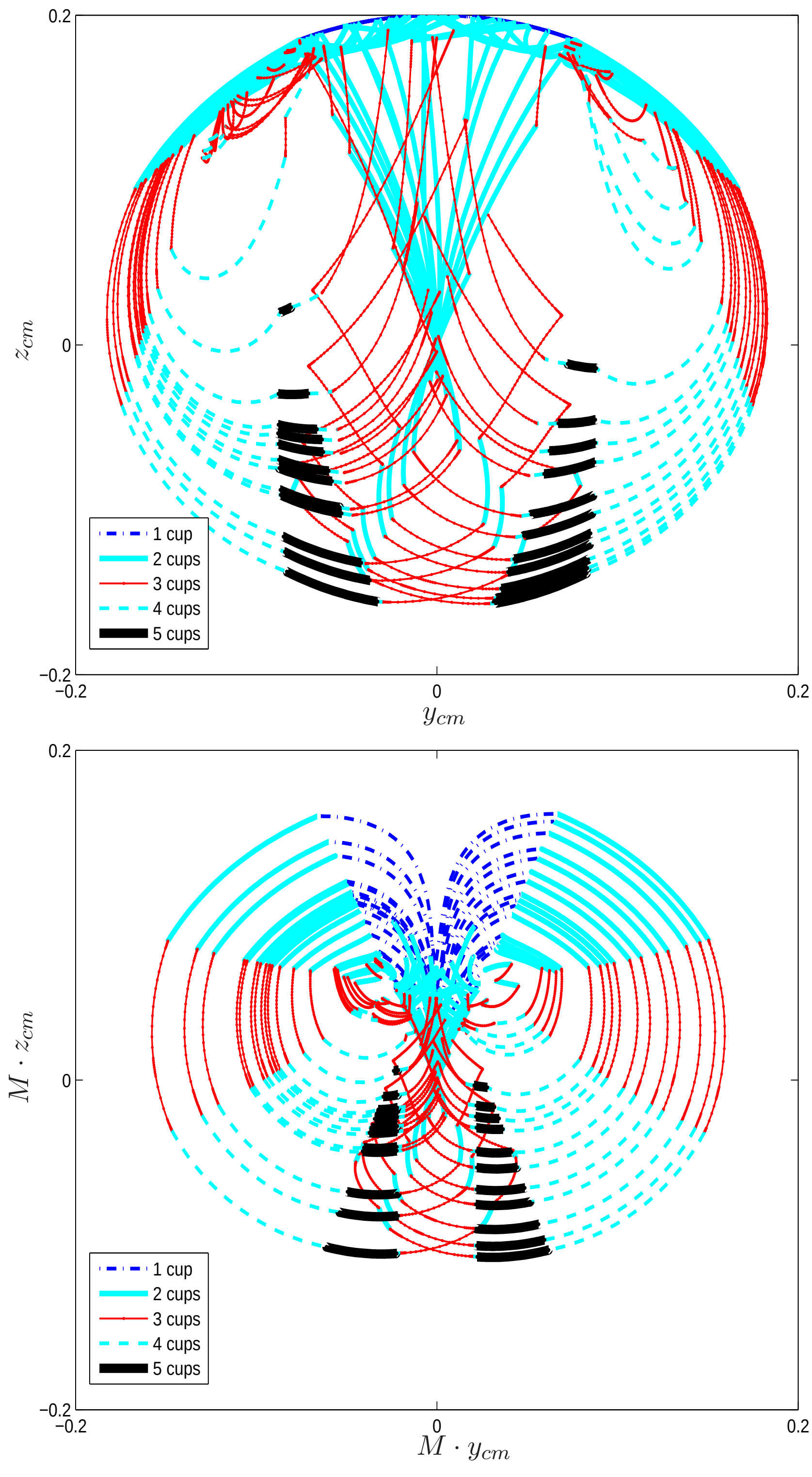

FIG. 2: (color online). The top panel is a center of mass trajectory for the sandwheel attractor according to Eq. (4) and Eq. (7). The bottom panel is a trajectory of the product of total mass and center of mass. Both take $Q_s = 0.2$ for time from 2000 to 2400 seconds.

time series of z_{cm} vs. y_{cm} from the sandwheel solution with $Q = 0.2\,kg \cdot s^{-1}$. A connection with the classic Lorenz-type butterfly figure is not immediately apparent. What is striking, however, is the segmentation of the trajectory into spatial regions largely delineated by the magnitude of γ, the number of non-empty cups. This suggests that γ is an important measure of the system in the case of small Q_s, since the dynamics of the sandwheel are visually correlated with the variability of γ. We mentioned that the waterwheel reaches a fixed mass $M_w = Q/K_w$ after some transient phase, which is not the case with the sandwheel. If we take the system to a constant γ, we can claim waterwheel dynamics for that parameter regime of the sandwheel. In the lower panel of Fig. 2, a modified center of mass plot is presented for the same parameter values as the panel above, where the center of mass quantities have been multiplied by the current total mass in system. Now the Lorenz butterfly is obvious, as is the segmentation. The difficulty in observing the butterfly in the top panel suggests that the steady state mass assumption is an important but subtle feature in plots like those of Strogatz and Matson. In the rest of this paper, we will use modified center of mass plots to describe the sandwheel, like the bottom panel of Fig. 2. These modified coordinates, which are related to the Fourier coefficients and which take into account the possibly variable total mass in the system, allows us to better compare and contrast the behavior of the waterwheel and sandwheel.

There is an intuitive understanding of the trajectory we are looking at in both panels of Fig. 2, which is perhaps easier to see in the top panel. When the majority of the system's mass is contained in one cup, that cup quickly reaches the bottom of the wheel and rotation ω slows. At this point the center of mass is near the bottom of the wheel. As the filled cup empties, the cup opposite to the bottom cup fills at the top of the rim. This causes the center of mass to rise through the center of the wheel. It is at this point when the direction of the next turn depends more on slight perturbations. Local Lyapunov exponents are higher in this region.[11] As the upper cup overtakes the lower one, the wheel spins one way or another and ω increases again. For this particular set of parameters, only one or two cups have any sand in them at this point. But as the wheel spins more cups get sand, as shown in the increase of the sum of all the Heaviside functions, γ. Once again the dominating cup reaches the bottom, and the process is repeated. Figure 2 portrays the dynamics of the modified center of mass of the sandwheel in a way that can be easily recognized by those familiar with Lorenzian systems, although the trajectories are interestingly partitioned by the number of active cups. However, it is not the dynamics of a given set of parameters where the differences are most noticeable, but when we study the transitions of well-known bifurcation parameters.

The top panel of Fig. 3 presents the bifurcation diagram of the waterwheel when Q_w is used as the bifurcation parameter. The study of Kolmogorov Entropy shows how the mere calculation of the exponent of the distance in diverging trajectories is a good approximation to the maximum Lyapunov exponent (this is, provided we do it in time intervals with a corresponding trajectory that is small relative to the radius of its curvature).[13,14] Thus, the panel below the bifurcation diagram shows this estimate for the maximum Lyapunov exponent (denoted λ_{max}), allowing us to recognize the transition to chaos and back to periodicity, as it was discussed in Becerra-Alonso.[11] The periodicity of low Q is different from that in high Q. For small values of Q, the waterwheel always rolls in the same direction (a permanent orbit in one of the two sides of the corresponding Lorenzian attractor). On the other hand, large values of Q (in Fig. 3) make the waterwheel turn back and forth like a pendulum (the fixed orbit now goes to both sides of the attractor). In between these two there is chaos, where positive Lyapunov exponents are found within this interval.

Figure 4 contains plots of post-transient trajectories of the center of mass at six values of Q_w as labeled in the first column by (a) through (f), ranging in value from 0.0265 to 1.3 $(kg \cdot s^{-1})$. Just to the right of each trajectory is a grayscale plot indicating relative mass of each of the cups through time in seconds. The cup with the most water at a given time is represented in black, while empty cups are white. All cups with mass in between these two are plotted in gray. The specific values of Q are [0.0265 (a), 0.0445 (b), 0.0460 (c), 0.0596 (d), 0.3798 (e), 1.3 (f)] in $kg \cdot s^{-1}$, and the motivation for these particular values of Q will become clear later. The top row of panels corresponds to four Q values from the clearly periodic regime of the bifurcation diagram ($Q < 0.1$), the middle row of panels to the chaotic region (Q roughly between 0.1 and 1.2) and the last to the quasiperiodic phase ($Q > 1.2$). Notice that the sequence of trajectories in the top panel of Fig. 4 and corresponding to Q values (a) through (d) appear to move towards the origin monotonically for a very small increase in Q, although a computation shows an increase in rotational inertia. When Q becomes larger than about 1.2, the system enters a stable nearly periodic pendulum-like motion. It first rotates in one direction, then the other, but never overturning and therefore never unstable. This compliments well the evidence of the bifurcation diagram and spectrum, and lends

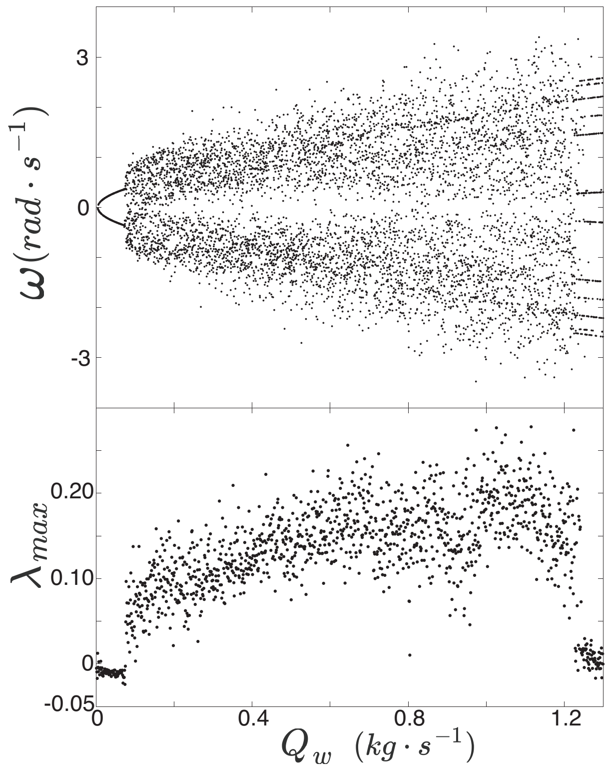

FIG. 3: Bifurcation diagram (top) and Lyapunov spectrum (bottom) of the waterwheel according to Eq. (1) and Eq. (7).

intuition about the physical reasons for these changes of state.

However, we find a completely different set of transitions in the sandwheel. Chaos and periodicity in the sandwheel follow a quite unexpected pattern and an array of dynamics not known in the waterwheel. In order to explain each one of these dynamics, we present a bifurcation diagram and approximate Lyapunov spectrum in Fig. 5. Figure 6 contains a series of panels detailing specific trajectories of the modified center of mass, and individual relative mass for each. The specific values of Q are [0.17 (a), 0.24 (b), 0.3 (c), 0.4 (d), 0.6 (e), 0.8 (f)] in $kg \cdot s^{-1}$, as given in the first column. As before, the cup with the most sand at a given time is plotted in black, while empty cups are in white. All cups with mass in between these two are plotted in gray.

A closer look at different regions in the Fig. 5 gives us an array of the different dynamics. For $Q = 0.17$ (a) we find a particular case where the system tends to converge to a periodic rolling, either clockwise or counterclockwise. For values of Q near this periodic regime (particularly $Q = 0.24$ (b)), we find chaos that appears closest to the Lorenzian form as

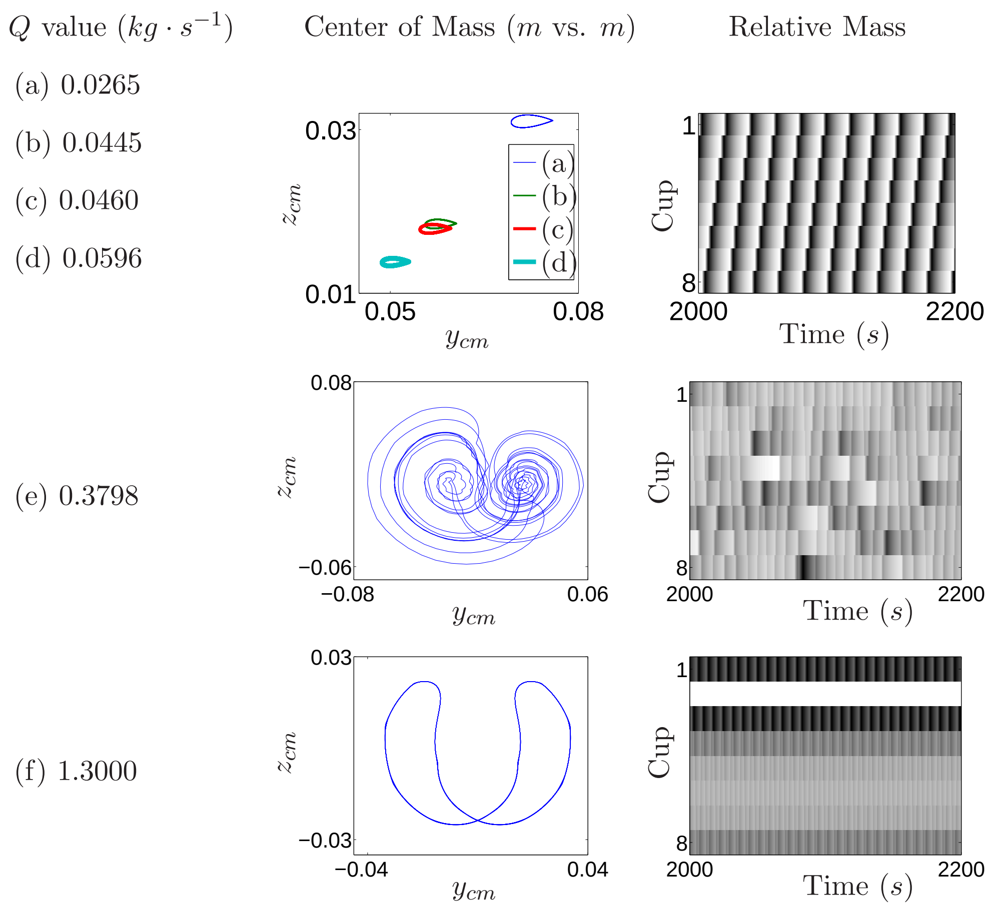

FIG. 4: Waterwheel sample trajectories of center of mass (middle column) and grayscale of relative mass in active cups (last column) for specific Q values (first column).

it is presented most typically (with the Prandtl number close to $\sigma = 10$ and the Rayleigh number close to $R = 28$). Figure 1 is an example of parameters in this region. For higher values of incoming sand ($Q = 0.3$ (c)) the system oscillates quasiperiodically between two values. For $Q = 0.4$ (d) the noise is gone and all that remains is periodicity. The grayscale plot confirms that this is the case. From this point (e) the system enters a regime beginning near $Q > NK_s \approx 0.72$. Just as it happened in (c) the Heaviside effect is abundant here, and noise takes over. Heaviside seems to act in waves of resonance with respect to Q. Noise in the grayscale plot in (e) disguises what the modified center of mass plot shows: overall Lorenzian topology is preserved. But this grayscale plot is far from comparable with that of (b), the first parameter region in which chaos is observed. Finally, $Q = 0.8$ (f), the return to periodicity, is actually the result of what happens when $Q > NK_s$. The system saturates, and sand grows without bound. Periodic behavior is the only way the sandwheel

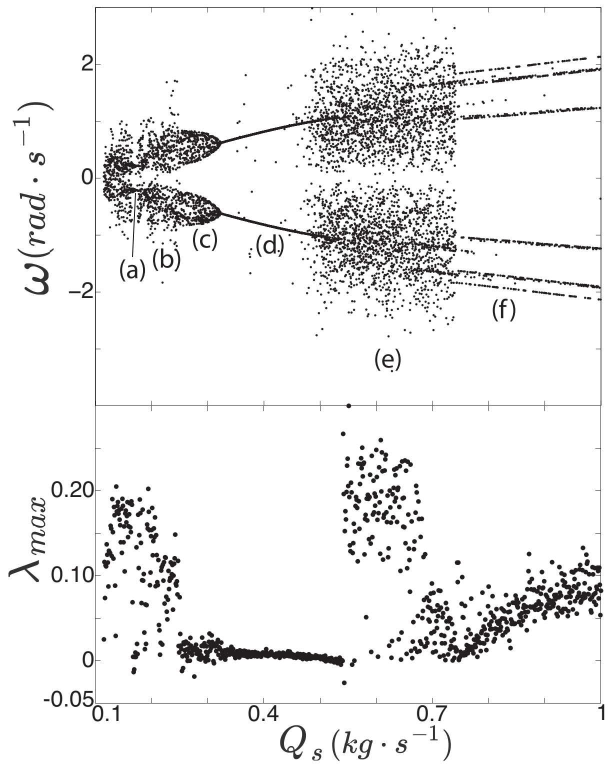

FIG. 5: Bifurcation diagram (top) and Lyapunov spectrum (bottom) of the sandwheel according to Eq. (4) and Eq. (7).

can deal with the system from this point. Even if at this point we forced an upper limit to the amount of sand the system can manage, the dynamics would still remain the same: rolling back and forth in a stable orbit. The grayscale plot shows very well this extreme, while the modified center of mass plot shows the saturation after a transient. The modified center of mass orbit is slowly converging towards a periodic orbit where the mass of each cup is growing unbounded.

The grayscale plots to the right of Fig. 6 allude to another interesting aspect of the sandwheel. Recall that γ is the number of non-empty cups in the sandwheel and increases from $\{1, 2\}$ cups in (a) to approximately 5 cups in (b) and (c). The range of γ is within $\{6, 7\}$ cups in (e). The progressive increase of the number of active cups in the sandwheel makes the dynamics resemble those of the waterwheel, since all cups are active in the waterwheel setting.

A direct comparison of bifurcation parameters, Q_s and Q_w, in the two bifurcation diagrams is difficult. The direct relationship between Q_w and M_w, however, can be used to get

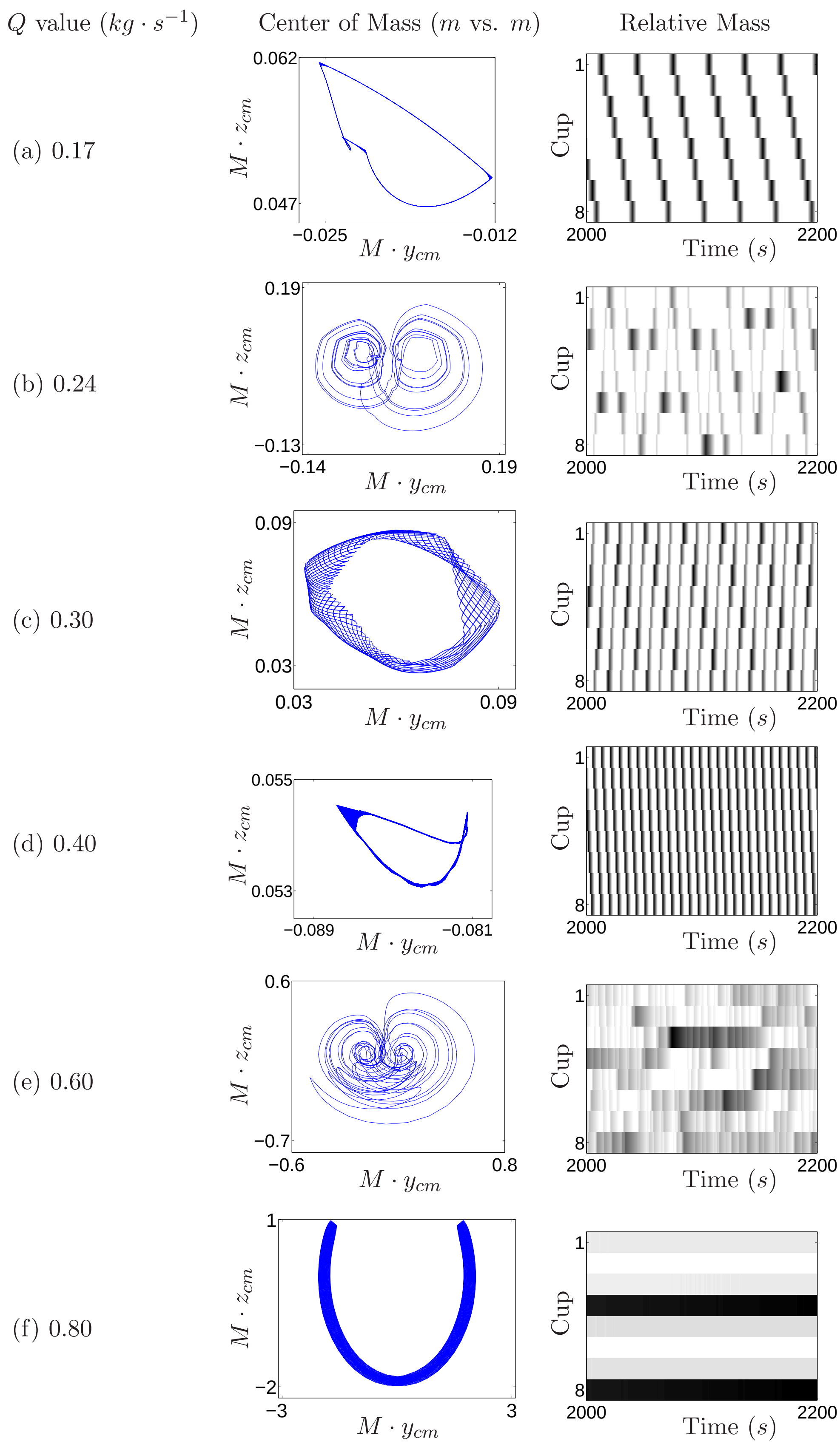

FIG. 6: Sandwheel sample trajectories of modified center of mass (middle column) and grayscale of relative mass in active cups (last column) for specific Q values (first column).

a relative picture. By first fixing Q_s, then computing a time averaged total mass of the sandwheel, as sampled uniformly over $t \in [2000, 2200]$ seconds and denoted by $\bar{M}_s$, an equivalent Q_w can be recovered from $\bar{M}_s = Q_w/K_w$ for comparison in the waterwheel setting. It is for this reason that the values of Q_w were selected in Fig. 4, as an attempt to compare the behavior of the two system using total (average) mass as bifurcation parameter, rather than the more typical Q. The largest value of $Q_s = 0.8$ has no direct analog in the waterwheel setting because the mass in this case does not reach a steady state. Using this method, it appears that $Q_s \in [0.1, 0.5]$ maps to the periodic regime of the waterwheel, ($Q_w \in [0, 0.1]$). This suggests that the transition on regions (a) through (d) in Fig. 5 is driven by γ, and that at times γ provides a large enough perturbation to drive the trajectory away from a single lobe of the attractor, when the modified center of mass is sufficiently close to origin of the center of mass (in Fig. 5 regions (a)-(b) and Fig. 6(a-b)). This chaotic perturbation knocks the system into a chaotic trajectory, attracted to both lobes of the Lorenzian attractor. At other times it appears that γ is not quite large enough to disrupt the Lorenzian dynamics sufficiently to force the attractor out of the attraction region, but is still large enough to result in quasiperiodicity in (c) (and in Fig. 6c). Even in the perturbed periodic region of (d), γ still occasionally (but rarely) is able to push the system away from the attracting manifold, but not to the competing lobe of the attractor.

IV. SUMMARY

The numerical approach shows that the discontinuity introduced by the Heaviside function does not completely distort the essential dynamics found in the waterwheel. Still, it severely affects the routes to chaos common to the waterwheel, and the parameter spaces where these transitions occur. Although the introduction of the Heaviside function makes analysis much more complicated, neither the topology of the center of mass, nor the dynamics are in the most fundamental sense severely affected. The sandwheel looks like a waterwheel when rotating. No sharp turns or unexpected movements are found beyond those of the chaotic waterwheel. It is simply complemented by permanent perturbations induced by γ that only slightly reshape the center of mass attractor.

The detailed dynamics of the sandwheel have shown a much richer array of behaviors than seen in the waterwheel. We find the two forms of periodicity and chaos, just as they are found in the waterwheel. But the sandwheel also presents quasi-periodicity and a border of chaos unique in that it is associated with the region where incoming sand dominates leaking sand. This threshold was predicted in the analysis prior to simulation. Then, numerical results showed the transition to be not as sharp. Instead the return to periodicity in the sandwheel (as we increase Q) happens more as a struggle of overloaded cups against almost empty ones. Periodicity finally takes over when the same cups finally retain a positive balance of sand after every turn of the wheel.

The parameter regimes for different dynamics are redefined when compared to those of the waterwheel. There is periodicity in the midst of two large intervals of chaotic regimes. The chaotic sandwheel extends the dynamics of Malkus' waterwheel with the addition of γ, a discrete feature. It appears, from a comparison based on total mass of the system, that γ has a large influence on dynamics for low total mass of the system, and triggers chaotic dynamics in regions that would be periodic in a sandwheel continuous setting, but has progressively less impact as total mass grows. What makes the sandwheel appealing is that the magnitude of this effect is self-regulating. While the Lorenzian dynamics that lie at the heart of the waterwheel analysis still appear in the sandwheel, the dynamics are sufficiently different and require a more in-depth theoretical analysis.

Acknowledgments

This work was partially supported by the MAA-NREUP, NSF-DMS-0552763, and NSA-H98230-06-1-0156. The authors thank Drs. Brian Utter and Paul Warne for helpful discussions, and Dr. David Laroze for his assistance and advice on the Lyapunov exponents measurement. Thanks to the editor and the reviewers of this article who made excellent suggestions and greatly improved this paper.

[1] E.N. Lorenz, "Deterministic nonperiodic flow", J. Atmos. Sci., **20**, 130–141 (1963).

[2] H. Haken, "Analogy between higher instabilities in fluids and lasers", Phys. Lett. A, **53**, 77 (1975).

[3] E. Knobloch,"Chaos in the segmented disc dynamo", Phys. Lett., **82A**, 439–440 (1981).

[4] W.V.R. Malkus, "Non-periodic convection at high and low Prandtl number", Mem. Soc. R. Sci. Liege Collect, **IV**, 125–128 (1972).

[5] S.H. Strogatz, *Nonlinear Dynamics And Chaos: With Applications To Physics, Biology, Chemistry, And Engineering*, Studies in Nonlinearity (Perseus Books Group, 1994).

[6] M. Kolár and G. Gumbs, "Theory for the experimental observation of chaos in a rotating waterwheel", Phys. Rev. A, **45**, 626-637 (1992).

[7] F. Gassmann, "Noise-induced chaos-order transitions", Phys. Rev. E, **55**, 2215–2221 (1997).

[8] A. Clauset, N. Grigg, M. Lim, and E. Miller, "Chaos you can play in", *SFI CSSS 2003 Proceedings* (2003).

[9] A.A. Mishra and S. Sanghi, "A study of the asymmetric Malkus waterwheel: The biased Lorenz equations", Chaos, **16**, 013114 (2006).

[10] L.E. Matson, "The Malkus-Lorenz water wheel revisited", Am. J. Phys., **75**, 1114-1122 (2007).

[11] D. Becerra-Alonso, *Deterministic Chaos in Malkus' Waterwheel: A simple dynamical system on the verge of low-dimensional chaotic behaviour*, (Lambert Academic Publishing, 2010).

[12] L. Illing, R.F. Fordyce, A.M. Saunders, R. Ormond, "Experiments with a Malkus-Lorenz water wheel: Chaos and Synchronization", Am. J. Phys, **80**, 192-202 (2012).

[13] G. Benettin, L. Galgani, and J. Strelcyn, "Kolmogorov entropy and numerical experiments", Phys. Rev. A, **14**, 2338–2345 (1976).

[14] W.G. Hoover and H.A. Posch, "Direct measurement of Lyapunov exponents", Phys. Lett. A, **113**, 82–84 (1985).